Thermophysical and tribological properties of dispersions based on graphene and a trimethylolpropane trioleate oil

José M. Liñeira del Río[a], María J. G. Guimarey[a], María J. P. Comuñas[a], Enriqueta R. López[a,*], Alfredo Amigo[b], Josefa Fernández[a]

[a]Laboratory of Thermophysical Properties, Nafomat Group, Department of Applied Physics, Faculty of Physics, University of Santiago de Compostela, 15782, Santiago de Compostela, Spain

[b]Laboratory of Thermophysical and Superficial Properties of liquids, Department of Applied Physics, Faculty of Physics, University of Santiago de Compostela, 15782, Santiago de Compostela, Spain

Journal of Molecular Liquids 268 (2018) 854-866

https://doi.org/*10.1016/j.molliq.2018.07.107*

*Corresponding author.

E-mail address: enriqueta.lopez@usc.es (E. R. López)

Abstract

The objective of this work is to study the tribological and thermophysical properties of nanolubricants composed by a trimethylolpropane trioleate (TMPTO) oil, and graphene nanoplatelets (GnP). For this aim, nanolubricants based on TMPTO with 0.05, 0.10, 0.25 and 0.50 wt% of graphene nanoplatelets were prepared. The dependence on temperature and concentration of the viscosity, density and speed of sound was determined by means of a rotational viscometer and two mechanical oscillation densimeters. Likewise, the antifriction and antiwear properties of these nanolubricants were analyzed. For this purpose, tribological tests were carried out at room temperature in a tribometer operating in ball on plate configuration and in reciprocating mode under a working load of 2.5 N. A 3D optical profilometer was used to analyze the wear track through the width of the scar. As regards thermophysical behavior of density and viscosity, both increase as the concentration of nanoparticles increases, whereas the speed of sound slightly diminishes when the GnP concentration increases. The best antifriction-antiwear performance was obtained for the nanolubricant containing 0.25 wt% in GnP.

Keywords: Density; viscosity; speed of sound; friction; wear; graphene; biodegradable oil

1. Introduction

With the advent of nanotechnology, new nanomaterials have been the aim of research as lubricant additives because of their unusual properties [1-5]. There are many different types of nanomaterials with potentially interesting antifriction and antiwear properties [1, 2, 6-9]. Among them, different carbon-based nanomaterials are being subject of interest [2]. In this regard, in recent years graphene is object of research as lubricant additive because it has much better thermal conductivity, reduced friction capacity and anti-wear properties compared to those of other nanoadditives [10, 11]. The most remarkable progress on graphene based nanofluids and nanolubricants has been recently collected in a review [11]. The first conclusion of this review is that graphene nanoflakes can significantly enhance the thermophysical and tribological properties of base oils and coolants. Nevertheless, the authors point out that in order to understand the interaction of graphene flakes with contact surfaces, detailed tribological studies are required [11].

Graphene nanoplatelets (GnPs) are carbon nanostructures consisting of small stacks of graphene sheets, having thickness in the range from 1 nanometer up to a few tens of nanometers, and lateral linear dimensions varying from a few micrometers up to hundreds of micrometers [12]. Most of the research involving dispersions of GnPs are focusing in the field of heat transfer [11, 13], thus the property most studied is the thermal conductivity. Literature on viscosity is scarce. Moghaddam *et al.* [14] reported rheological properties of graphene-glycerol nanofluids, finding that the viscosity of the nanofluids rises with the increase of graphene mass fraction. These authors also found a very strong shear thinning behavior. Dhar *et al.* [15] found that the viscosity of nanosuspensions of graphene nanosheets in water increases with concentration and decreases with temperature. Mehrali *et al.* [10] studied the rheological behavior of dispersions of GnPs in distilled water. Sadeghinezhad *et al.* [16] analyzed the temperature and concentration dependences of the viscosity of aqueous dispersions of GnP; from their work it is shown that viscosity increases with the loading of the GnP nanoparticles

due to the increase in friction and flowing resistance of fluids. Azman *et al.* [17] evaluated the effects of GnPs as additives in palm-oil trimethylolpropane (TMP) ester blended in polyalphaolefin, finding that the increase in the GnP concentration resulted in increasing values of viscosity, density and viscosity index. Vakili *et al.* [18] determined the viscosity of nanofluids containing GnP and deionized water from 20 to 60 ºC, at concentrations ranging from 0.025 to 0.10 wt% of GnP finding also that viscosity increases when GnP concentration rises. Iranmanesh *et al.* [19] investigated the effect of GnP/distilled water nanofluids on the thermal performance of evacuated tube solar collector in solar-water heater systems. For this purpose, these authors measured physical and thermal properties of the GnP nanofluids including viscosity. The results showed Newtonian behavior. At constant temperature, viscosity rises with GnP concentration, which the authors attribute to the increase of the resistance of the fluid flow due to the high specific surface area of the GnP nanosheets. Rashmi *et al.* [20] have found viscosity increases up to 168% for dispersions of GnP in an additivated palm oil trimethylolpropane ester lubricant.

As regards the tribological behavior of nanolubricants containing GnPs, Eswaraiah *et al.* [21] prepared ultrathin-graphene based engine oil nanofluids evaluating their frictional characteristics, antiwear, and extreme pressure properties, obtaining improvements compared with the base oil of 80%, 33%, and 40%, respectively. Bernan *et al.* [22] found that small amounts of few-layer-graphene-containing ethanol solution strongly decreased wear and friction coefficients respect to neat ethanol. Guo and Zhang [23] investigated multi-layered graphene (5-8 layers) as additive of a polyalphaolefin (PAO2), with a four-ball test method, finding that the friction reduction and anti-wear ability of pure lubricant was improved, showing the 0.05 wt% graphene dispersion the better tribological properties. Azman *et al.* [17] also obtained that the addition of 0.05 wt% GnP in blended lubricant resulted in both lowest coefficient of friction and wear scar diameter, with reductions of 5 and 15% respectively, comparing with the blended lubricant. Rasheed *et al.* [24] studied nanolubricants formulated using graphene nanoflakes and two engine oils found that the addition of 0.01 wt% graphene to one of these oils results in 23%

enhancement and 21% reduction in thermal conductivity and in the friction coefficient, respectively. Wu *et al.* [25] investigated, using a four-ball testing machine, the tribological behavior of two types of tribopairs (Si_3N_4/GCr15, GCr15/GCr15) lubricated with an aviation lubricant with few layer graphene as additive. For the second tribopair these authors found that the friction coefficient and the wear scar diameter decreased 25% and 39%, respectively, with the addition of 0.05 wt% to the neat oil. The addition of 0.075 wt% in the same neat oil resulted in the reductions of friction coefficient and wear scar diameter of 27% and 43%, respectively. Rashmi *et al.* [20] achieved a maximum reduction of 7% and 16% for the coefficient of friction and the wear scar diameter, respectively, with the introduction of 0.05wt% of GnPs in the additivated palm oil trimethylolpropane ester. Finally, Kiu *et al.* [26] studied the effect on tribological properties of the addition of carbon-based nanoparticles as lubricant additives of a vegetable oil; the nanoparticles investigated were graphene nanosheets (GN), carbon nanotubes, and graphene oxide. The results showed that the most positive effect in improving the tribological properties of the neat oil is obtained with the addition of 50 ppm GN.

In this paper we have characterized thermophysical properties of nanodispersions based on GnP and an ester type lubricant: a trimethylolpropane trioleate (TMPTO) based oil. This ester has excellent lubricating properties [27], high viscosity index [28], is nonflammable and biodegradable in an 80% or more [29]. For this purpose, densities, viscosities and the speed of sound in the different dispersions have been measured at atmospheric pressure as a function of temperature. In addition to evaluate the antifriction and antiwear properties of the dispersions, tribological test were performed under a load of 2.5 N.

2. Experimental section

2.1 Materials

The base oil used in this work was kindly provided by Croda. The sample was characterized by infrared spectroscopy (IR). This oil can be identified as trimethylolpropane trioleate (TMPTO, CAS: 57675-44-2), its chemical structure is shown in Fig. 1. The FTIR spectrum of TMPTO (Fig. 2) shows a strong peak at 1741 cm^{-1}, which can be assigned to the stretching vibration of ester carbonyl (C=O), a peak at 1157 cm^{-1} which corresponds to (C–O–C) single bond stretching vibration, a peak at 722 cm^{-1} due to the alkyl chains of TMPTO and peaks of carbon–hydrogen (C–H) stretching and bending which are observed at 2922–2853 cm^{-1} and 1463 cm^{-1} [30, 31].

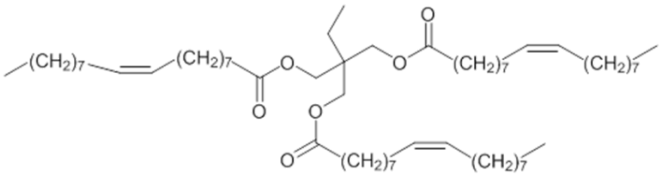

Fig. 1. Trimethylolpropane trioleate structure

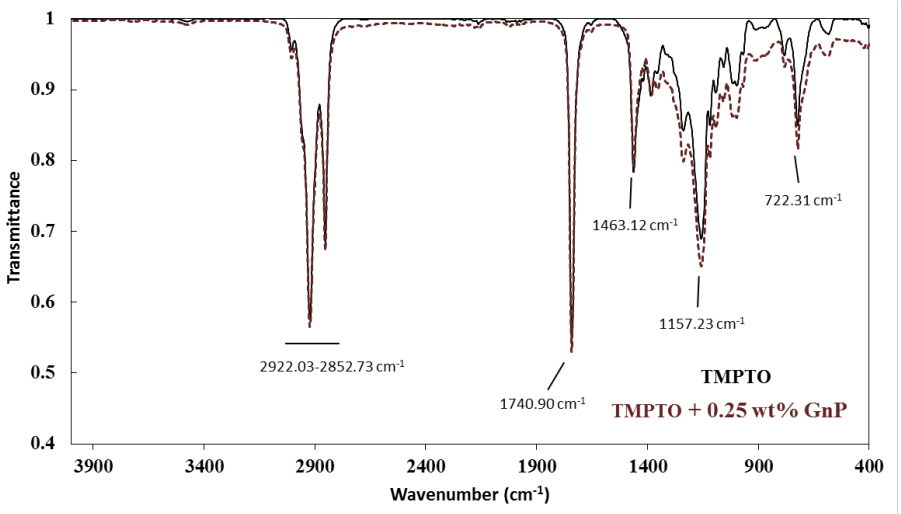

Fig.2. FTIR spectrum of TMPTO (-) and of the 0.25 wt% GnP nanodispersion (···)

In addition, the base oil was also characterized by means of high performance liquid chromatography, HPLC, coupled to a quadrupole orthogonal acceleration time-of-flight mass

spectrometer (micrOTOF-Q™) equipped with an electrospray ionization source (ESI). The sample was dissolved in isopropanol (5:200) and analyzed by isocratic mode, being the injection volume 5 μL. The time of the analyses was 30 minutes, with a flow of 0.7 ml/min and using methanol and isopropanol in 0.1% like aqueous phase. The chromatogram (Fig. 3) shows three identified peaks that correspond to the components of the sample, and others that correspond to the pattern sample analysis. The mass spectrum (Fig. 4) of the majority compound, corresponding to peak 3, shows that the mass of the molecular ion coincides with that of TMPTO (molecular mass 927.51 $g \cdot mol^{-1}$). The mass spectra of the other two components of the oil (Figures S1 and S2 of the Supplementary Information) indicate that their molecular masses are around 925 and 923 $g \cdot mol^{-1}$. Taking into account these results and the FTIR spectrum we can conclude that the second and third compounds of the base oil have the same structure as TMPTO but with two and four hydrogen atoms less, this fact could correspond to one (peak 2) or two (peak 1) C=C bonds instead C-C bonds. Therefore, our base oil is composed by 68.3% of TMPTO, 27.6% of a compound with a C=C bond more than TMPTO and a 4.1% of a compound with two C=C bonds more than TMPTO.

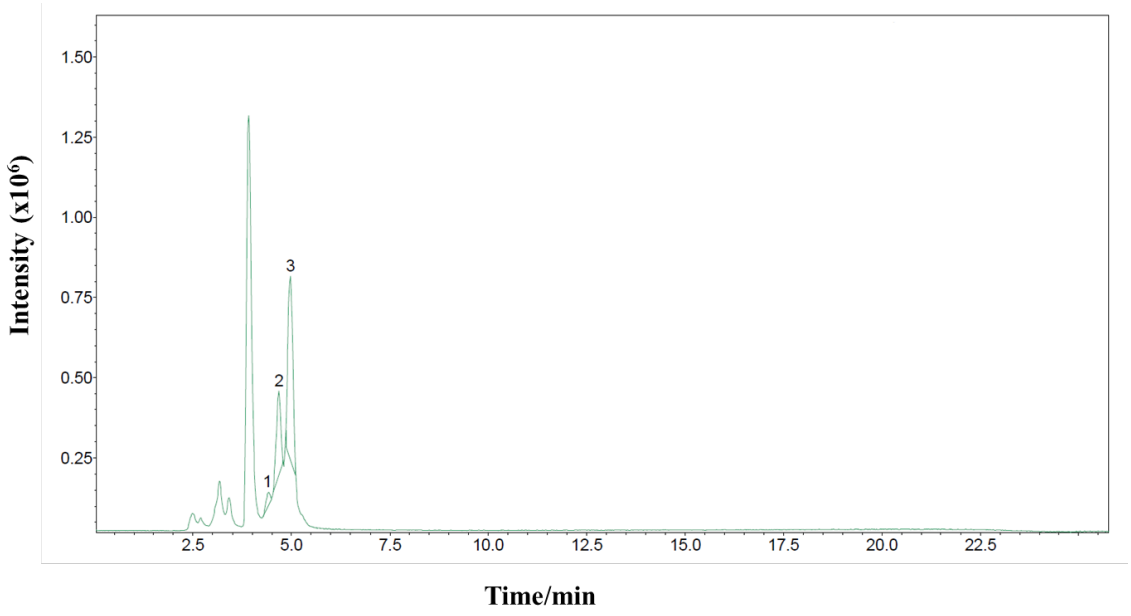

Fig. 3. HPLC chromatogram of the TMPTO sample.

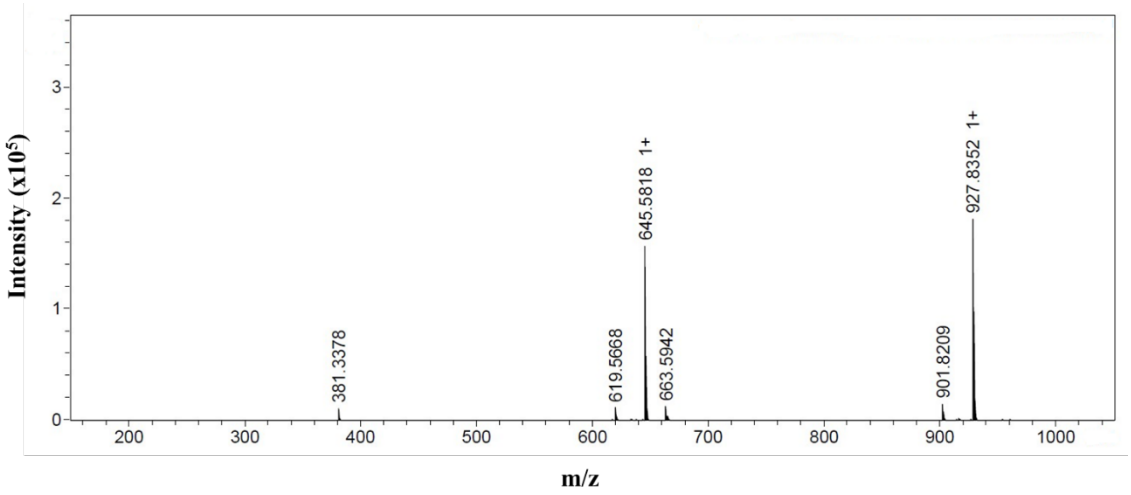

Fig. 4. Mass spectrum of TMPTO (component 3 in Fig. 3). Retention time 5.0 min.

Graphene nanoplatelets (GnP, CAS number 1034343-98-0) of a purity of 99.5% with an average particle diameter of 15 μm and of 11-15 nm of thickness, were provided by Iolitec. In order to analyze their morphology and size, the nanoplatelets were characterized by both transmission and scanning electron microscopy (TEM and SEM). SEM micrographs were taken with a Zeiss Ultraplus Field Emission Scanning Electron Microscope, FESEM. TEM images were carried out with a JEOL JEM-2010 equipment; for this purpose, nanoparticles were dispersed in 1-butanol. Detailed images of the specimen are shown in Figs. 5 and 6. The appearance of GnP shows that platelets are bend and wrinkled.

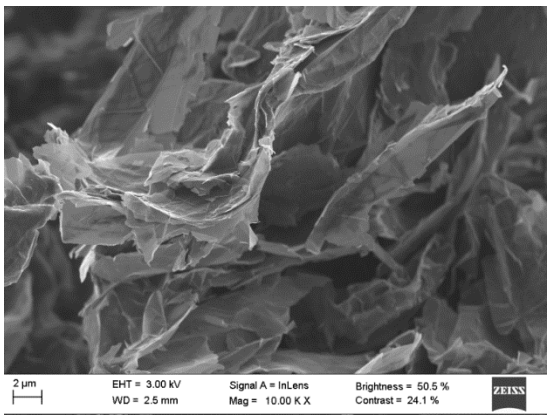

Fig. 5. SEM image of GnP

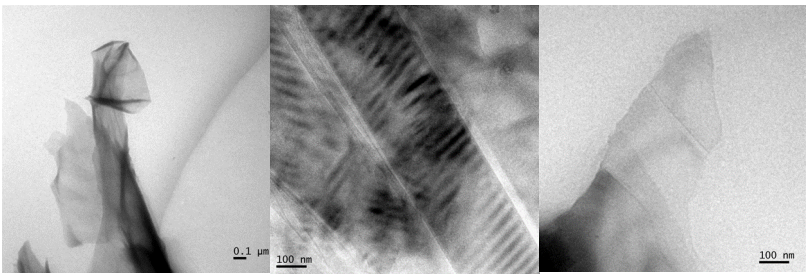

Fig. 6. TEM images: structure of aggregates of GnP previously dispersed in 1-butanol

The FTIR spectrum (Fig. 7) shows a peak at 3333 cm^{-1} which is attributed to O-H stretching vibrations, an absorption peak at 2920 cm^{-1} indicating the C-H stretching, and a weak peak at 1658 cm^{-1}, which refers to C=O stretching vibrations. A quite wide and intense peak appears at 1453 cm^{-1} which corresponds to O–H bending vibrations. Several absorption peaks were observed at around 1152 to 1024 cm^{-1}, indicating the presence of C-O stretching of alcohol [32, 33]. Therefore, due to the nature of the graphene borders, one of the major impurities are oxygen-containing groups. Carbonyl and hydroxyl groups are usually impurities due to the reaction synthesis of GnP [33]. EDX analysis shows an atomic composition of GnP with more than 95% carbon.

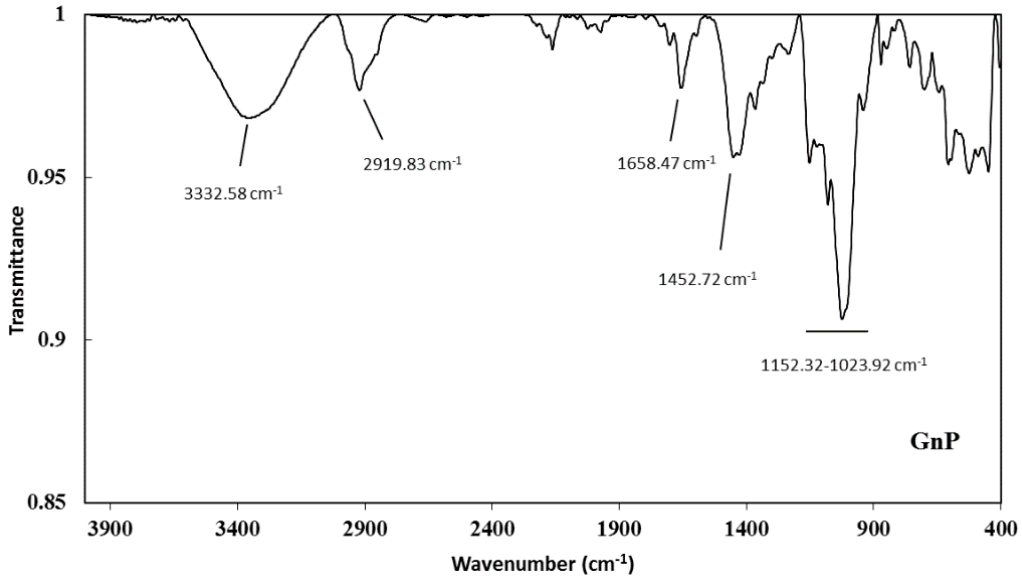

Fig. 7. The FTIR spectrum of graphene nanoplatelets

Raman spectroscopy in the visible range, specifically at a wavelength of 514 nm, was used in order to characterize the graphene nanoplatelets (Fig. 8), since this technique is a powerful non-destructive tool to characterize carbonaceous materials. The typical characteristics for graphene carbon in Raman spectra for visible excitation are the D-band which lies at 1350 cm^{-1}, the G-band around 1580 cm^{-1} and the second order of the D-band (2D) which is also called G´-band and appears around 2700 cm^{-1} (Fig. 8). All of these bands can change in shape, position, or relative intensity and so reflect the evolution of the graphene structure and its electronic properties [34]**.** The G peak is due to the bond stretching of all pairs of sp^2 atoms in both rings and chains while the D peak is a result of the breathing modes of sp^2 atoms in rings, finally the 2D peak is caused by the double resonant Raman scattering with two-phonon emissions [35, 36]. Graf and Molitor [37] analyzed the change of G band with different number of graphene layers, indicating that the intensity of the G band increases in an almost linear relation when the number of layers grows. This is possible because the more layers of graphene, the more sp^2 bond carbon atoms being detected by the laser spot [38]. The G' peak in Raman spectra of graphene is also a useful tool to find the number of layers, in this case when a single peak appears, graphene consists on a single-layer; the increase in the G' band width can be associated with a higher number of graphene layers [38]. As it can be seen in the following spectrum (Fig. 8), our graphene nanosheets correspond to a multilayer type due to the high intensity of the G-band, as well as the pronounced width of the G'-band.

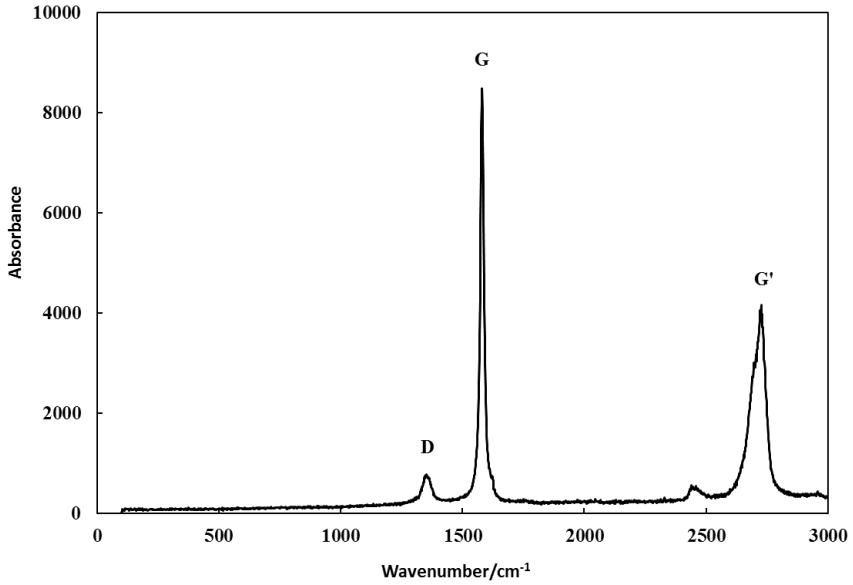

Fig. 8. The Raman spectrum of graphene nanoplatelets

2.2 Samples preparation

Nanodispersions with different concentrations of GnP (0.05, 0.10, 0.25 and 0.50 wt%) in the base oil were prepared. Two-step method was used to prepare the nanolubricants. Firstly, mixing the GnP dry powder with the base oil (TMPTO), for this stage, a Sartorius balance (model MC 210P) with a readability of 0.01 mg, was used. At the second step the homogenization of the samples has been carried out with a Fisherbrand ultrasonic bath, with continuous shaking periods of 4 hours and at a shaking frequency of 37 kHz. The comparison between the FTIR spectrum of the base oil and that of the 0.25 wt% dispersion of graphene is presented in Fig. 2. It is clear that there are no new chemical interactions between the TMPTO oil and the graphene nanoplatelets.

In order to check the stability of the dispersion, the visual observation was used. The nanodispersions with the smallest and the biggest compositions were checked. Signs of sedimentation seem to appear later than 96 h after sonication (Fig. 9). ~~This time is longer than the necessary to perform the thermophysical and tribological studies (around six hours).~~ Additional stability tests of the nanodispersions were performed using a Zetasizer Nano ZS (Malvern Instruments) based on dynamic light scattering technique (DLS). We must point out

that the studied nanoadditives are sheet-like shaped, whereas DLS technique is based on the assumption that particles are spherical. The experiments were made for the nanodispersion of 0.25 GnP mass concentration at 298 K in the backscattering mode (collection angle 173°). The procedure consists in keeping the sample undisturbed during the test time (around 150 h in this work) in order to evaluate changes in size distribution due to nanoparticle sedimentation or flocculation. Figure 10 reveals agglomeration of GnP nanoadditives in the nanodispersions. Thus, an average diameter around 627 nm was obtained. We observe that this value remains almost constant over the test time. This fact is in agreement with the visual observation and confirms that the nanodispersions are stable during an interval time much longer than that necessary to perform the thermophysical and tribological characterization (around six hours).

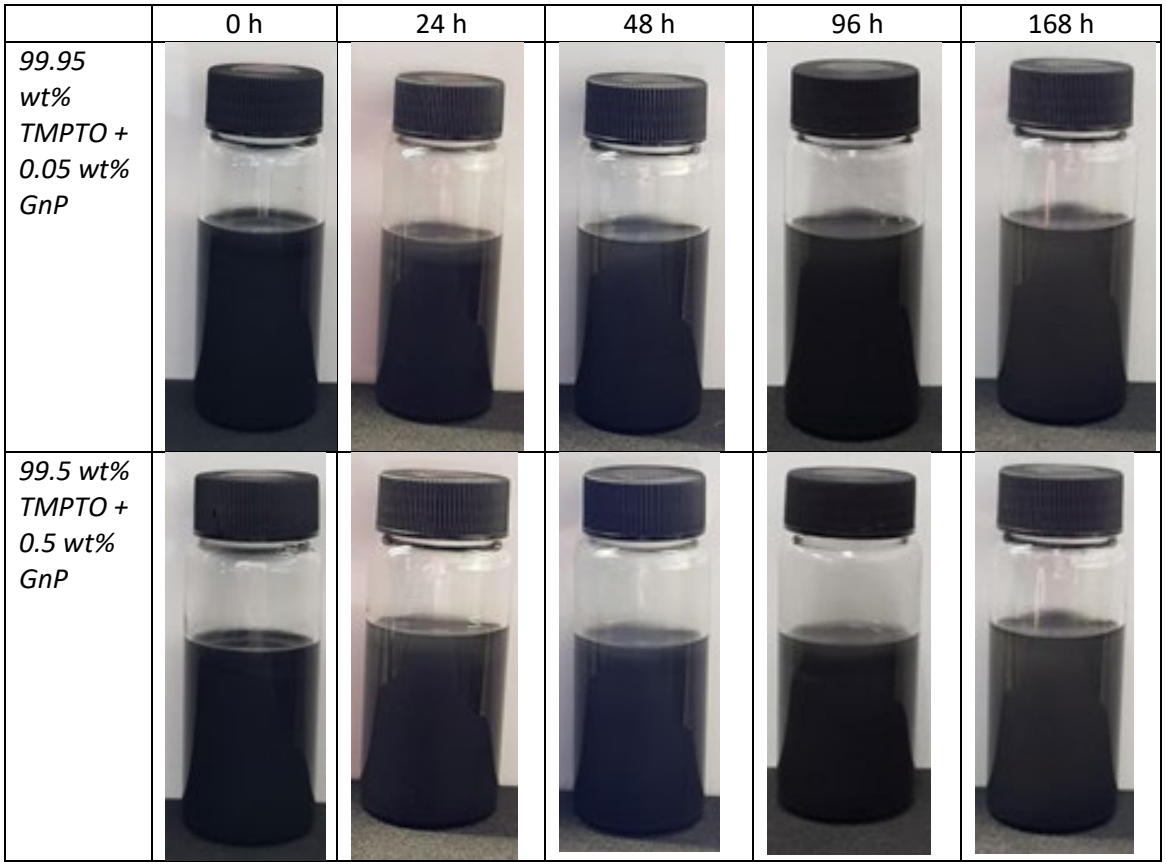

Fig. 9. Stability of the nanodispersions: visual temporal evolution.

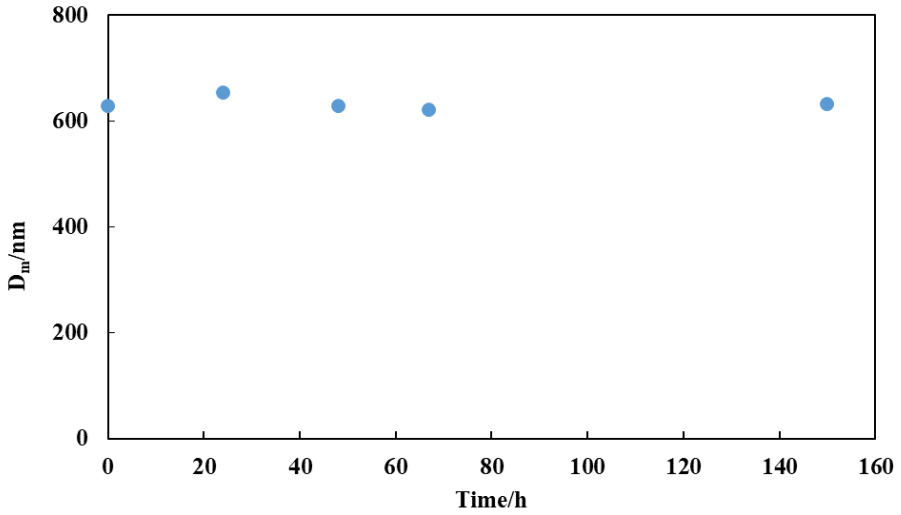

Fig. 10 Temporal evolution of apparent average particle size, D_m, obtained by DLS for the 0.25 wt% GnP/TMPTO nanodispersion.

2.3 Thermophysical Characterization

An automated SVM 3000 Anton Paar rotational Stabinger viscometer [39] which includes a vibrating tube densimeter was used to determine the viscosity and density of the pure oil and the nanolubricants at atmospheric pressure. Details of this equipment have been reported previously [40, 41]. Dynamic viscosity and density were determined over the temperature range of 278.15 K to 373.15 K at atmospheric pressure. The expanded uncertainties (k=2) are 0.02 K for temperature, 0.0005 g·cm^{-3} for density and 1 % in the case of dynamic viscosity. The Stabinger SVM 3000 viscometer has a measurement mode that provides the value of the viscosity index according to ASTM D2270 standard.

Speed of sound in the temperature range 283.15 to 338.15 K were determined, with an expanded uncertainty of 1 m·s^{-1}, by using an Anton Paar DSA 5000. This equipment also allows to determine density with an expanded uncertainty of 1·10^{-5} g·cm^{-3}. The temperature is kept constant within 0.005 K. The use of both, the Stabinger SVM 3000 and Anton Paar DSA 5000 allows to check the consistency of density measurements.

2.4 Tribological Tests

Reciprocating friction tests were carried out using a CSM Standard tribometer in a ball-on-plate configuration [28]. Chrome steel balls AISI 52100 (diameter: 6 mm; hardness: 803 HV) were run against AISI 420 stainless steel plates (40.5 × 21 × 5 mm^3; hardness: 194 HV) with a mirror finish polishing (roughness lower than 11 nm). All the plates were cleaned with hexane and dried in air before the tests. The plates were lubricated with five drops of the lubricant. Tests were conducted at room temperature (~296 K) under a normal load of 2.5 N that corresponds to a maximum contact pressure of 0.88 GPa. At least three replicates were performed for each sample at a stroke length of 10 mm, maximum speed of 0.10 $m \cdot s^{-1}$ and a sliding distance of 500 m. After each tribological test, the specimens were rinsed with a stream of hexane for a few seconds.

Wear was evaluated in terms of the width of the wear scar by means of a 3D Optical Profiler Sensofar S Neox. For these measurements, we have worked in confocal mode with a 10X objective for all lubricants analyzed. We also have done a stitching operation in order to get the full images of wear scar. SEM images were conducted on the worn surface to examine its morphology. These analyses were performed on the Zeiss FESEM ULTRA Plus Scanning Electron Microscope with integrated EDX detectors.

3. Results and Discussion

3.1. Thermophysical Properties

The experimental densities obtained with the SVM 3000 and DSA 5000 devices for the pure oil and for the nanolubricants are presented in Tables 1 and 2. An average absolute deviation (AAD% [42]) of 0.04% was found between both sets of values, which is in agreement with the combined uncertainty of both devices. As usual, for a fixed concentration, densities decrease when the temperature rises (6.7% in the studied temperature range). In addition, this property

slightly increases with the concentration of nanoparticles in the dispersion. Therefore, an average increase of 0.29% is reached at the highest composition analyzed (0.50 wt% in GnP) as can be observed in Fig. 11. Thus, when the number of nanoparticles per unit volume increases, the particles agglomerate causing the nanofluid density to increase [43].

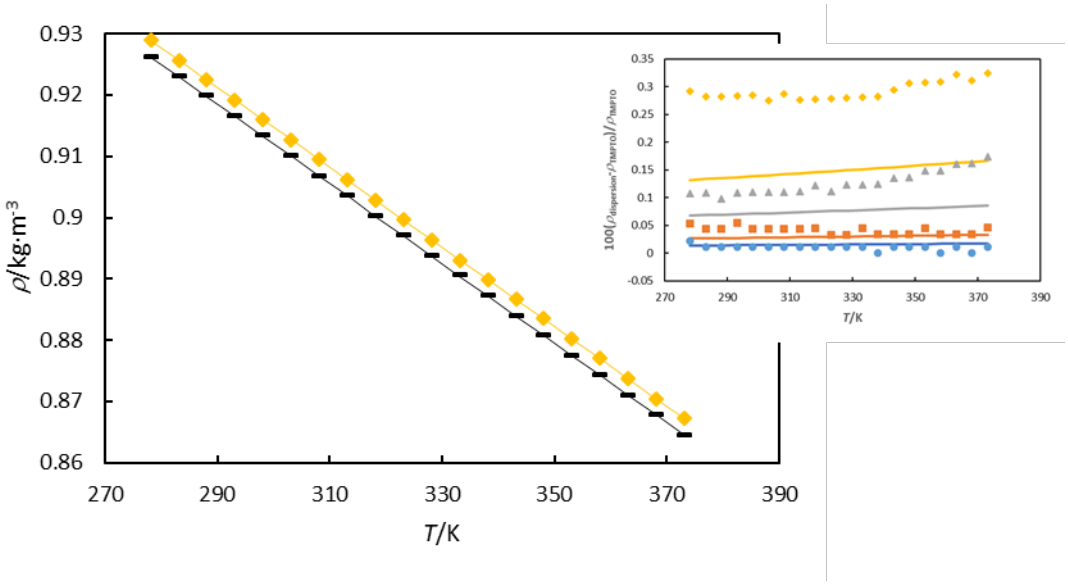

Fig. 11. Density of TMPTO (-) and the nanolubricant with the highest composition (♦) as a function of temperature. Solid lines represent the correlation (Eq. 1). Inset: relative increase of the density of the nanolubricants in relation to the base oil as a function of temperature. GnP concentration: (●) 0.05 wt%, (■) 0.10 wt%,(▲) 0.25 wt% and (♦) 0.50 wt%. Solid lines represent the relative deviations of the predictions of the Pak and Cho model (Eq. 2).

Table 1

Density, ρ/g·cm^{-3}, of the dispersions TMPTO + GnP as a function of temperature at 0.1 MPa obtained with the Anton Paar Stabinger SVM 3000

T/K	ρ/g·cm^{-3}	T/K	ρ/g·cm^{-3}	T/K	ρ/g·cm^{-3}
		TMPTO			
278.15	0.9263	313.15	0.9037	348.15	0.8808
283.15	0.9231	318.15	0.9004	353.15	0.8775
288.15	0.9199	323.15	0.8972	358.15	0.8743
293.15	0.9166	328.15	0.8939	363.15	0.8710
298.15	0.9134	333.15	0.8906	368.15	0.8678
303.15	0.9102	338.15	0.8874	373.15	0.8645
308.15	0.9069	343.15	0.8841		
		99.95 wt% TMPTO + 0.05 wt% GnP			
278.15	0.9265	313.15	0.9038	348.15	0.8809
283.15	0.9232	318.15	0.9005	353.15	0.8776
288.15	0.9200	323.15	0.8973	358.15	0.8743
293.15	0.9167	328.15	0.8940	363.15	0.8711
298.15	0.9135	333.15	0.8907	368.15	0.8678
303.15	0.9103	338.15	0.8874	373.15	0.8646
308.15	0.9070	343.15	0.8842		
		99.90 wt% TMPTO + 0.10 wt% GnP			
278.15	0.9268	313.15	0.9041	348.15	0.8811
283.15	0.9235	318.15	0.9008	353.15	0.8779
288.15	0.9203	323.15	0.8975	358.15	0.8746
293.15	0.9171	328.15	0.8942	363.15	0.8713
298.15	0.9138	333.15	0.8910	368.15	0.8681
303.15	0.9106	338.15	0.8877	373.15	0.8649
308.15	0.9073	343.15	0.8844		
		99.75wt% TMPTO + 0.25 wt% GnP			
278.15	0.9273	313.15	0.9047	348.15	0.8820
283.15	0.9241	318.15	0.9015	353.15	0.8788
288.15	0.9208	323.15	0.8982	358.15	0.8756
293.15	0.9176	328.15	0.8950	363.15	0.8724
298.15	0.9144	333.15	0.8917	368.15	0.8692
303.15	0.9112	338.15	0.8885	373.15	0.8660
308.15	0.9079	343.15	0.8853		
		99.50 wt% TMPTO + 0.50 wt% GnP			
278.15	0.9290	313.15	0.9062	348.15	0.8835
283.15	0.9257	318.15	0.9029	353.15	0.8802
288.15	0.9225	323.15	0.8997	358.15	0.8770
293.15	0.9192	328.15	0.8964	363.15	0.8738
298.15	0.9160	333.15	0.8931	368.15	0.8705
303.15	0.9127	338.15	0.8899	373.15	0.8673
308.15	0.9095	343.15	0.8867		

Table 2

Density, ρ/g·cm^{-3}, of the TMTPO and the dispersions TMPTO + GnP as a function of temperature at 0.1 MPa obtained with the Anton Paar DSA 5000.

T/K	ρ/g·cm^{-3}	T/K	ρ/g·cm^{-3}	T/K	ρ/g·cm^{-3}
			TMPTO		
283.15	0.923047	303.15	0.909809	323.15	0.896587
288.15	0.919756	308.15	0.906492	328.15	0.893297
293.15	0.916439	313.15	0.903186	333.15	0.890021
298.15	0.913124	318.15	0.899884	338.15	0.886747
			99.95 wt% TMPTO + 0.05 wt% GnP		
283.15	0.923230	303.15	0.909930	323.15	0.896776
288.15	0.919941	308.15	0.906680	328.15	0.893483
293.15	0.916627	313.15	0.903374	333.15	0.890201
298.15	0.913309	318.15	0.900072	338.15	0.886820
			99.90 wt% TMPTO + 0.10 wt% GnP		
283.15	0.923442	303.15	0.910207	323.15	0.896991
288.15	0.920155	308.15	0.906897	328.15	0.893702
293.15	0.916839	313.15	0.903585	333.15	0.890418
298.15	0.913523	318.15	0.900289	338.15	
			99.75 wt% TMPTO + 0.25 wt% GnP		
283.15	0.924268	303.15	0.911036	323.15	0.897880
288.15	0.920975	308.15	0.907723	328.15	0.894531
293.15	0.917667	313.15	0.904428	333.15	0.891249
298.15	0.914349	318.15	0.901114	338.15	0.887973
			99.50 wt % TMPTO + 0.50 wt% GnP		
283.15	0.925576	303.15	0.912352	323.15	0.899131
288.15	0.922287	308.15	0.909037	328.15	0.895847
293.15	0.918980	313.15	0.905729	333.15	0.892567
298.15	0.915667	318.15	0.902425	338.15	0.889290

An empirical equation was used to correlate the densities of Table 1, ρ, of TMTPO and TMPTO + GnP dispersions [44]

$$\rho = A + BT + Cw \tag{1}$$

where w is the percentage weight content of GnP in the nanodispersion and *A*, *B* and *C* are adjustable parameters. As can be observed in Fig. 11, Eq. (1) excellently correlates the experimental values despite its simplicity. Thus, an AAD of 0.011 % and maximum deviation of 0.031 % were obtained.

Experimental densities of the nanodispersions, ρ_{nd}, have been compared with those predicted by the Pak and Cho model [45]:

$$\rho_{nd} = (1-\phi)\rho_f + \phi\rho_{np} \quad (2)$$

where ϕ, the volume fraction of GnP was determined through the equation

$$\phi = \frac{m_{np}/\rho_{np}}{m_{np}/\rho_{np} + m_f/\rho_f} \quad (3)$$

The subscript *f* refers to the neat oil whereas *np* does to the nanoparticles. The value of 2.25 g·cm^{-3} for ρ_{np} of GnP was used [46]. AADs between density values estimated with equation (2) and those experimentally determined with Stabinger SVM 3000 range from 0.03% for the nanolubricants containing a 0.0064 wt% of GnP, up to 0.14% for the 0.50 wt% composition were obtained. This model underestimates the density values of the nanodispersions with the three highest compositions.

We have also compared experimental densities of the nanodispersions with those provided by Wasp *et al.* [47] predictive equation:

$$\rho_{nd} = \frac{1}{(1-\varphi)/\rho_f + \varphi/\rho_{np}} \quad (4)$$

being φ the mass fraction of the nanoparticles in the solution. In this case AADs between density values estimated with equation (3) and those experimentally determined with Stabinger SVM 3000 range from 0.060% for the dispersion with the lowest content in GnP to 0.15% for the highest composition. Thus, similar results were found with this equation than with the previous one. This model also underestimates the density values of the nanodispersions for GnP concentrations of 0.1, 0.25 and 0.50 wt%.

Assuming a quadratic temperature dependence of the experimental densities, isobaric thermal expansion coefficients, α_p, for the nanodispersions have been evaluated from their definition:

$$\alpha_p = -\frac{1}{\rho}\left(\frac{\partial \rho}{\partial T}\right)_p \tag{5}$$

In Fig. 12 we present several isotherms of α_p as a function of the volume fraction of GnP. It is observed that α_p increases when the temperature rises whereas it diminishes very slightly with particle loading. In addition, we have estimated this property using the following expression:

$$\alpha_{p,nd} = \phi \cdot \alpha_{p,np} + (1-\phi) \cdot \alpha_{p,f} \tag{6}$$

where $\alpha_{p,nd}$ is the isobaric thermal expansion coefficient of the nanodispersions, $\alpha_{p,np}$ is that of the of GnP which was taken from the literature [48], and $\alpha_{p,f}$ is that of the base fluid, in this case TMPTO. In Fig. 12 we have also plotted the estimated values using Eq. (6). Excellent agreement between the experimental and estimated values can be observed. The AADs are lower than 0.095% and the maximum deviation (0.11%) is obtained for the highest composition (0.50 wt% of GnP).

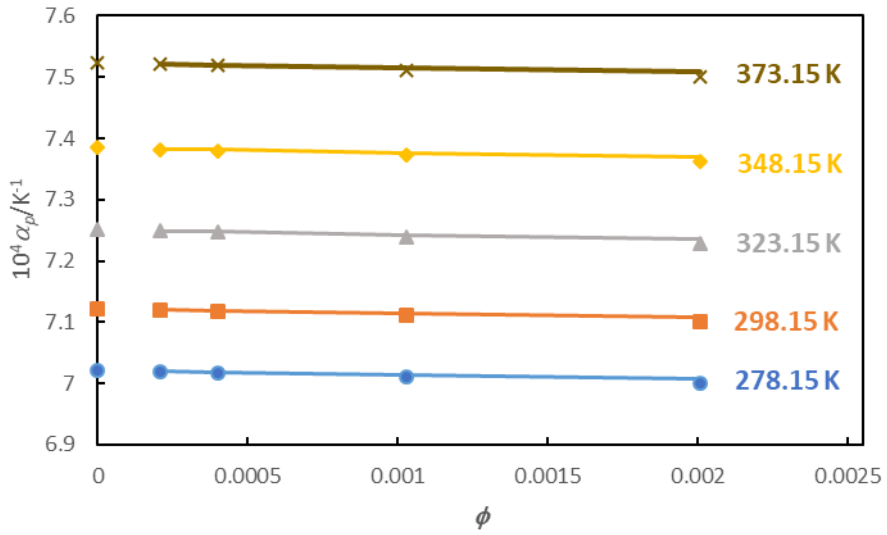

Fig. 12. Isobaric thermal expansion coefficients, α_p, of the nanodispersions against the volume fraction of GnP. Values obtained from experimental densities: (●) 278.15 K, (■) 298.15 K, (▲) 323.15 K, (♦) 348.15 K and (×) 373.15 K. Solid lines represent the estimated values (Eq 6).

The dynamic viscosities measured with the SVM 3000 device are reported in Table 3 for the TMPTO based oil and for the nanolubricants. As expected, viscosities decrease asymptotically when the temperature rises. As can be observed in Fig. 13, viscosities increase with the concentration of nanoparticles. Thus, relative increases up to 11.2 % are found for the base oil additivated with 0.50 wt% of GnP.

The effective thermophysical properties of nanofluids depend on those of the base fluid and the particle loading. Molecular dynamics simulations [49, 50] have shown that nanofluids are more ordered than the base fluid. Thus, the increase in the effective viscosity due to increasing particle concentration obeys to an increase in the degree of order of the fluid. In addition, Kannaiyan *et al.* [43] indicate that reducing viscosity when temperature rises is due to the weakening of Van der Waals forces and other secondary intermolecular bonds.

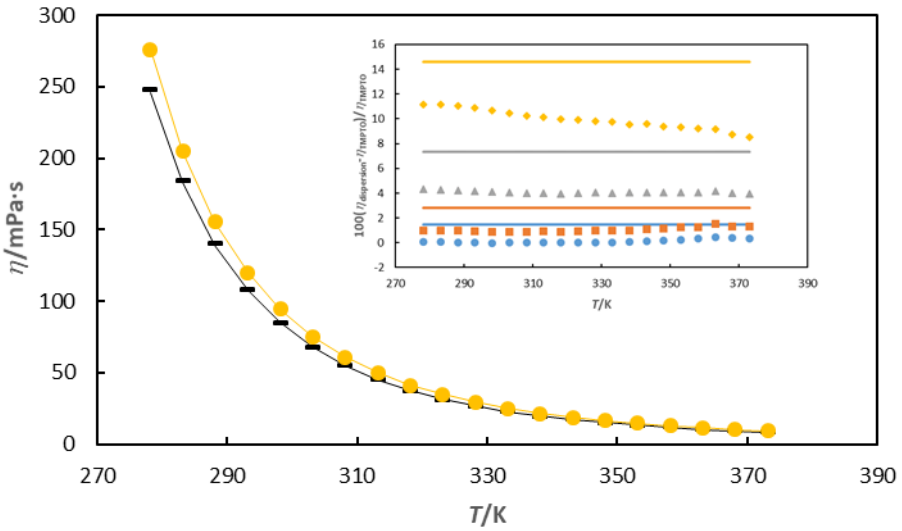

Fig. 13. Viscosity of TMPTO (-) and the nanolubricant with the highest composition (♦) as a function of temperature. Solid lines represent the correlation (Eq. 10). Inset: relative increase of the viscosity of the dispersions in relation to the base oil as a function of temperature. GnP concentration: (●) 0.05 wt%, (■) 0.10 wt%, (▲) 0.25 wt% and (♦) 0.50 wt%. Solid lines represent the relative deviations of the predictions of the Pak and Cho model [45] (Eq. (11)).

Table 3

Viscosity, η/mPa·s, of the dispersions TMPTO + GnP as a function of temperature at 0.1 MPa obtained with the Anton Paar Stabinger SVM 3000.

T/K	η/mPa·s	T/K	η/mPa·s	T/K	η/mPa·s
		TMPTO			
278.15	247.9	313.15	45.24	348.15	15.10
283.15	184.5	318.15	37.57	353.15	13.33
288.15	140.2	323.15	31.54	358.15	11.84
293.15	108.5	328.15	26.75	363.15	10.56
298.15	85.30	333.15	22.91	368.15	9.501
303.15	68.09	338.15	19.79	373.15	8.578
308.15	55.14	343.15	17.22		
		99.95 wt% TMPTO + 0.05 wt% GnP			
278.15	248.1	313.15	45.24	348.15	15.13
283.15	184.6	318.15	37.57	353.15	13.36
288.15	140.2	323.15	31.55	358.15	11.88
293.15	108.5	328.15	26.76	363.15	10.61
298.15	85.28	333.15	22.92	368.15	9.536
303.15	68.09	338.15	19.80	373.15	8.607
308.15	55.14	343.15	17.24		
		99.90 wt% TMPTO + 0.10 wt% GnP			
278.15	250.3	313.15	45.65	348.15	15.27
283.15	186.3	318.15	37.90	353.15	13.50
288.15	141.6	323.15	31.83	358.15	11.99
293.15	109.5	328.15	27.01	363.15	10.72
298.15	86.06	333.15	23.13	368.15	9.626
303.15	68.70	338.15	19.99	373.15	8.691
308.15	55.63	343.15	17.41		
		99.75wt% TMPTO + 0.25 wt% GnP			
278.15	258.6	313.15	47.05	348.15	15.71
283.15	192.4	318.15	39.05	353.15	13.87
288.15	146.1	323.15	32.80	358.15	12.32
293.15	113.0	328.15	27.83	363.15	11.00
298.15	88.79	333.15	23.83	368.15	9.881
303.15	70.85	338.15	20.59	373.15	8.917
308.15	57.35	343.15	17.92		
		99.50 wt% TMPTO + 0.50 wt% GnP			
278.15	275.5	313.15	49.82	348.15	16.52
283.15	205.1	318.15	41.32	353.15	14.57
288.15	155.7	323.15	34.66	358.15	12.93
293.15	120.3	328.15	29.37	363.15	11.53
298.15	94.40	333.15	25.14	368.15	10.33
303.15	75.22	338.15	21.68	373.15	9.307
308.15	60.80	343.15	18.87		

In the case of dynamic viscosities, an equation based on the Vogel-Fulcher-Tammann (VFT) equation was used to correlate the data of each nanodispersion:

$$\eta_{nd} = \eta_0 \exp\left(\frac{DT_0}{T - T_0}\right) \tag{7}$$

where η_{nd} is the viscosity of the nanodispersion, η_0, D and T_0 are adjustable parameters. In Fig. 14 we present the values of the parameters obtained as a function of the mass fraction of the nanodispersion. As can be observed the dependence of both η_0 and T_0 on mass fraction of the nanodispersion are second order polynomial functions. An interesting result is that obtained for D, which results to be mass fraction independent. Then, we have modified Eq. (7) including explicitly the following mass fraction dependences for η_0 and T_0:

$$\eta_0 = E + Fw^2 \tag{8}$$

$$T_0 = G + Hw + Iw^2 \tag{9}$$

Accordingly, the eq. (7) can be re-written as

$$\eta_{nd} = \left(E + Fw^2\right)\exp\left(\frac{D\left(G + Hw + Iw^2\right)}{T - \left(G + Hw + Iw^2\right)}\right) \tag{10}$$

being D, E, F, G, H, I adjustable parameters. As can be observed in Fig. 12, Eq. (10) fits the data adequately, being the AAD 0.51% and the maximum deviation 2.3%. Fig. 13 shows the excellent agreement between the results obtained from Eqs. (8) and (9) and the η_0 and T_0 values obtained from the individual correlations using Eq. (7).

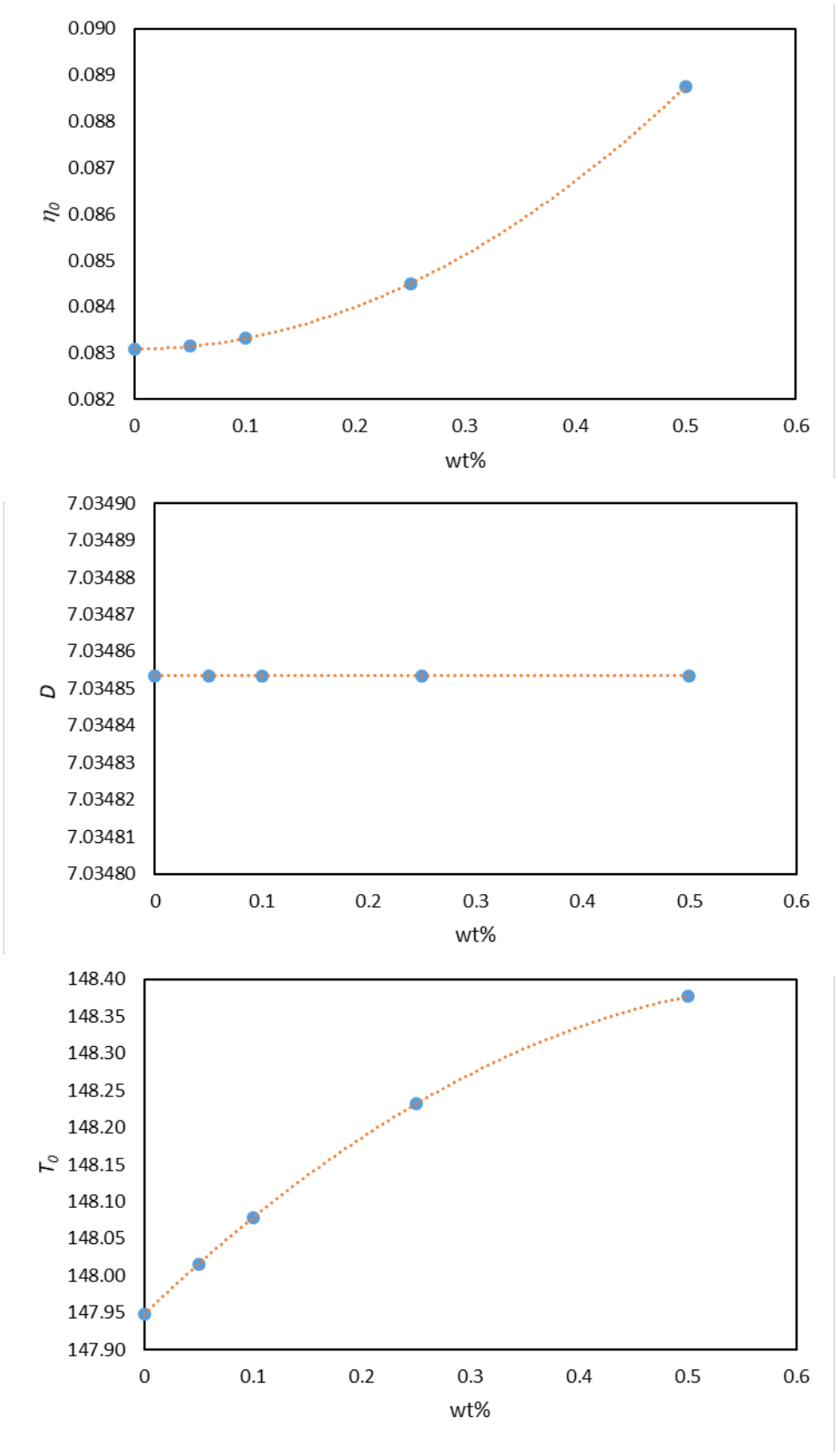

Fig. 14. Dependence on mass fraction of the nanodispersions of the parameters of Eq. (7). Dashed lines represent Eqs (8) and (9) and the *D* parameter in Eq. (10).

In the 1980s, Angell proposed a classification of liquids that form glasses according to their fragility [51], a concept that has since been very useful for the understanding of these systems. The concept fragility [41] can be used to classify fluids from their viscosity-temperature dependence. According to Angell's classification, liquids that form glasses called *strong* are characterized by weak discontinuities of their thermodynamic properties in the glass transition, and an almost-Arrhenius behavior of their transport properties as a function of the temperature, while the behavior for a *fragile* liquid is highly non-Arrhenius or also called super-Arrhenius behavior (the dependence on temperature is much stronger than that predicted by the Arrhenius equation). One way to evaluate whether a liquid is *fragile* or *strong* is through the Angell parameter (parameter *D* in Eq. (7)) [52, 53]. This parameter is great for *strong* liquids and is small for *fragile* liquids. In the present work a constant value of 7.0±0.1 was obtained, thus we can conclude that TMPTO is *fragile* and this behavior is unaffected by the GnP loading.

The obtained viscosity indexes are 190 for TMPTO and the 0.05 and 0.10 wt% dispersions and 188 and 184 for 0.25 and 0.50 wt% dispersions, respectively. Thus, this property remains approximately constant up to the composition of 0.25 wt% and then slightly decreases with concentration.

The reliability of three simple empirical predictive models has been examined through the experimental viscosity values of these nanodispersions. The first model is the Batchelor [54] equation:

$$\eta_{nd} = \eta_f \left(1 + 2.5\phi + 6.5\phi^2\right) \tag{9}$$

The second one was proposed by Chen *et al.* [55]

$$\eta_{nf} = \left(1 + 10.6\phi + (10.6\phi)^2\right)\eta_{bf} \tag{10}$$

In a previous work on thermophysical properties of nanofluids based on Zirconia [56], this equation showed reasonably agreement (absolute relative deviations lower than 4%) with the experimental viscosity data.

Finally, the empirical equation due to Pak and Cho [45]:

$$\eta_{nd} = \eta_f \left(1 + 39.11\phi + 533.9\phi^2\right) \quad (11)$$

Note that the three equations are second order polynomial functions of the nanoparticle volume fraction, ϕ, and do not provide an explicit temperature dependence of the viscosities but only an implicit one through the viscosity of the lubricant base, η_f. We have obtained that the first equation in the most of the conditions underestimates the viscosity with the only exception of the lowest GnP composition at which AAD% and bias% [42] are equal. AAD% values increase with the content in GnP of the dispersion being 8.2% the value at the highest composition. In the case of Eq. (10), AADs ranging from 0.29% for the lowest composition up to 5.5% for the highest ones were found. By the contrary Pak and Cho equation presents the best agreement with the experimental viscosity values being the AADs% lower than 4.2%. It is interesting to point out that when the slope of the predictive function increases, the predictions improve. The three models overestimate the viscosity values. In Fig. 13 the predictions obtained with the Pak and Cho model are presented in the inset.

The experimental speeds of sound in the pure oil and in the dispersions are reported in Table 4. Up to our knowledge there is no previous studies on speed of sound of nanodispersions involving GnPs. Speed of sound decreases linearly with increasing temperature for the TMPTO oil and the nanolubricants, which is the usual behavior for liquids [57]. As can be observed in Fig. 15, the speed of sound in the dispersions decreases very slightly (within the expanded uncertainty of the apparatus with which it was determined) with the concentration of nanoparticles. In order to propagate the sound, successive layers must be put into motion, and in liquids with strong bonds between molecules the transmission of the perturbation from one layer to the next will be facilitated [57, 58]. Thus, the practically insensitive tendency of the speed of sound with the GnP concentration confirms that there is no formation of chemical interactions between the neat oil and the nanoparticles; there are only physical interactions between nanoparticles and the neat oil.

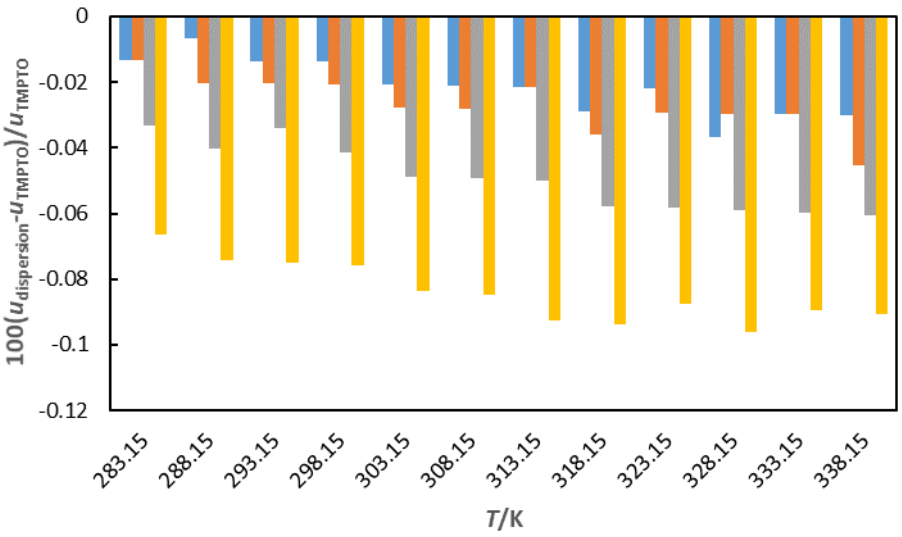

Fig. 15. Relative decrease of the speed of sound in the dispersions in relation to the base oil as a function of temperature. GnP concentration: (●) 0.05wt%, (■) 0.10 wt%, (▲) 0.25 wt% and (♦) 0.50 wt%.

Table 4

Speed of sound, u/m·s^{-1}, in the nanolubricants TMPTO + GnP at different temperatures and 0.1 MPa measured with the Anton Paar DSA 5000.

T/K	u/m·s^{-1}	T/K	u/m·s^{-1}	T/K	u/m·s^{-1}
		TMPTO			
283.15	1501.5	303.15	1434.1	323.15	1369.7
288.15	1484.4	308.15	1417.7	328.15	1354.1
293.15	1467.4	313.15	1401.5	333.15	1338.6
298.15	1450.6	318.15	1385.6	338.15	1323.3
		99.95 wt% TMPTO + 0.05 wt% GnP			
283.15	1501.3	303.15	1433.8	323.15	1369.4
288.15	1484.3	308.15	1417.4	328.15	1353.6
293.15	1467.2	313.15	1401.2	333.15	1338.2
298.15	1450.4	318.15	1385.2	338.15	1322.9
		99.90 wt% TMPTO + 0.10 wt% GnP			
283.15	1501.3	303.15	1433.7	323.15	1369.3
288.15	1484.1	308.15	1417.3	328.15	1353.7
293.15	1467.1	313.15	1401.2	333.15	1338.2
298.15	1450.3	318.15	1385.1	338.15	1322.7
		99.75 wt% TMPTO + 0.25 wt% GnP			
283.15	1501.0	303.15	14353.4	323.15	1368.9
288.15	1483.8	308.15	1417.0	328.15	1353.3
293.15	1466.9	313.15	1400.8	333.15	1337.8
298.15	1450.0	318.15	1384.8	338.15	1322.5
		99.50 wt% TMPTO + 0.50 wt% GnP			
283.15	1500.5	303.15	1432.9	323.15	1368.5
288.15	1483.3	308.15	1416.5	328.15	1352.8
293.15	1466.3	313.15	1400.2	333.15	1337.4
298.15	1449.5	318.15	1384.3	338.15	1322.1

A similar equation to that propose by Khanafer and Vafai [44] for densities (Eq. (1)) was used to correlate the speed of sound of TMPTO and the nanodispersions:

$$u_{nd} = A + BT + Cw \tag{12}$$

with A, B and C adjustable parameters. In this case an AAD of 0.064% and a maximum deviation of 0.17% were achieved. Thus, the fit standard uncertainty, 1.18 m·s^{-1}, is slightly higher than the experimental uncertainty (1 m·s^{-1}).

Isentropic compressibility, κ_s, was determined from the density and speed of sound measurements through the Newton-Laplace equation, $\kappa_S=1/(\rho u^2)$. The κ_s values increase when the temperature rises. In general, for the 0.05 wt% concentration the dispersions are more compressible than the neat oil, becoming less compressible when the concentration in GnP increases, which means that the free space volume decreases which is in agreement with the rise of density with the GnP concentration. As expected, the acoustic impedance, *Z*, determined from the speed of sound and density values, $Z=\rho u=(\rho/\kappa_S)^{1/2}$, presents an increasing trend with concentration.

3.2. Tribological Behaviour

The results obtained for the coefficient of friction (μ) can be seen in Fig. 16, for the tests performed with the neat base oil and with the nanolubricants with different percentages in weight of GnP, under a 2.5 N applied load. It can be clearly seen that the friction coefficient is reduced with respect to the pure oil for all the concentrations, having an optimal value for the dispersion of 0.50 wt% of GnP. Thus the lowest coefficient of friction is obtained, namely 0.105, for 0.50 wt% of GnP compared to 0.163 for the oil without additives. The relative reduction in the friction coefficient, $100\left(\left(\mu_{oil}-\mu_{dispersion}\right)/\mu_{oil}\right)$, calculated from the experimental values, ranges from 22% to 36%. Eswaraiah *et al.* [21] studied dispersions of graphene in engine oil finding that friction coefficients corresponding to all the nanodispersions were lower than that of the base oil. These authors attribute the improvement in the friction coefficient to graphene's layered structure and its self-lubrication. Other literature results on graphene nanoadditives also are explained through the formation of thin protective graphene layers between rough surfaces, thus improving the tribological properties of the neat oil [59].

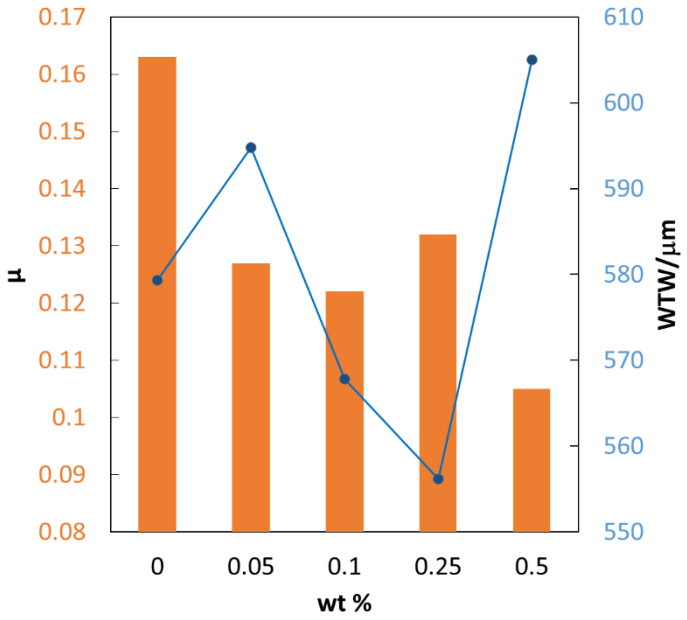

Fig. 16. Comparison between friction coefficient and wear obtained with the base oil TMPTO and with the nanolubricants. (■) Friction coefficient; (●) Maximum wear scar width.

An example of the wear tracks obtained is shown in Fig. 17. Optical micrographs were taken by means of the 3D Optical Profiler Sensofar S Neox. As can be observed the wear scar on the plate is wavy, indicating that there is plastic flow. This type of tracks has been previously observed [60-62]. In this regards Akagaki and Kato [60] have pointed out that in this case, the contact occurs partially at the early stage of friction, and then the wear scar consists of some wave-like streaks formed during the ploughing process.

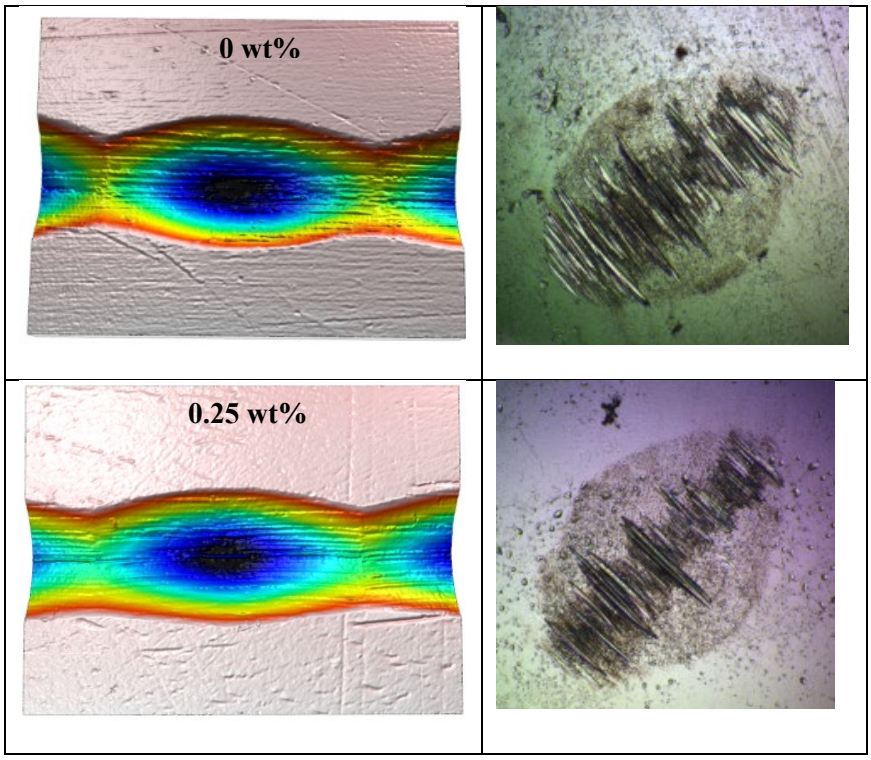

Fig. 17. Optical micrographs (10x) of a detail of the wear track on the plate and the balls, lubricating the contact with neat TMPTO and with the nanolubricant containing a 0.25 wt% of GnP.

The wear on the plates was evaluated in terms of the wear track width (WTW). Given the topography of these tracks (non-uniform), this measurement corresponds to the greatest width. In Fig. 16 we have plotted together with the friction coefficients, the maximum width of the wear tracks measured with a 3D Optical Profiler Sensofar S Neox. As can be seen in this figure, the WTW is reduced in relation to that obtained with the neat TMPTO oil, for the nanolubricants with 0.10 and 0.25 wt% in GnP. A potential lubricant must to protect sliding surfaces from wear and damage. Thus, although for this last composition the friction coefficient is not the minimum, wear is minimized, with a reduction of the wear scar width respect to that corresponding to the neat oil of 4%. Then we can conclude that the best antiwear and antifriction performance corresponds to this concentration, 0.25 wt%. Optimal concentrations for different nanodispersions were also found by other authors [23, 25, 26, 63-66]. Thus, Zin *et*

al. [64], Liu *et al.* [67] and Gupta *et al.* [66] indicate that for concentrations lower than the optimal ones, the amount of nanoparticles is insufficient to protect from wear. The higher the nanoparticle concentration, the larger the tendency to agglomerate. Agglomeration of particles may scratch the surface under loading and result in an increase of wear [23, 25, 64]. Thus, agglomeration caused by excessive content of nanoparticles is the possible reason for the increase of wear track depth at concentrations higher than the optimal ones.

SEM images have been taken for the worn scar obtained with the pure oil and with the dispersion with a 0.25 wt% in GnP at different magnifications (Fig. 18). As can be seen a slightly narrower and smoother surface can be observed in the case of the plate lubricated with the dispersion, showing the plate lubricated with TMPTO more ploughing, although no signs of severe abrasion are presented. We have measured with the 3D Optical Profile Sensofar S Neox the roughness of both worn surfaces to confirm the fact that the nanodispersion produces a smoother surface as compared to that of the neat TMPTO oil. The measured roughness parameter *Ra* was determined accordingly to the standard ISO 4287, applying a Gaussian filter with a long wavelength cut-off of 0.25 mm. A value of 83 nm was obtained for the worn surface lubricated with TMPTO whereas that for the scar corresponding to the 0.25 wt% in GnP dispersion was 48 nm. EDX analyses revealed a slight increase in the C content in the wear scar lubricated with the nanolubricant.

Several researchers have also found improvements in the antifriction-antiwear performances of lubricating oils when small quantities of GnP were added to the base fluid [11, 17, 21, 64]. Thus, for example, Azman *et al.* [17] have found an optimal concentration of 0.05 wt% GnP in a blended lubricant composed by palm-oil trimethylolpropane (TMP) ester and a polyalphaolefin (PAO10). Accordingly, these authors have found reductions of 5 and 15% in the coefficient of friction and wear scar diameter, respectively, when this dispersion is used instead of the blended lubricant.

For various types of tribological applications, the nanoparticle shape plays an important role [68]. The shape of nanoparticle depends on the pressure applied on the nanolubricants upon loading [68, 69]. The planar contact is the feature of nanoplatelets [68]. Thus, as Choudhar *et al.* [70] have suggested in their study about the dispersion of alkylated graphene in hexadecane, the supply of graphene nanosheets between the rubbing surfaces, improving the lubrication properties respect to the pure solvent. In the same regard, Kamel *et al.* [71] have found that the addition of graphene nanosheets in a lubricating grease could significantly reduce the interfacial friction and improve the load-bearing capacity of the parts. Thus, these authors attribute the excellent friction and anti-wear properties of graphene sheets to their extremely thin laminated structure, which offers lower shear stress and prevent interaction at the rubbing interface [71].

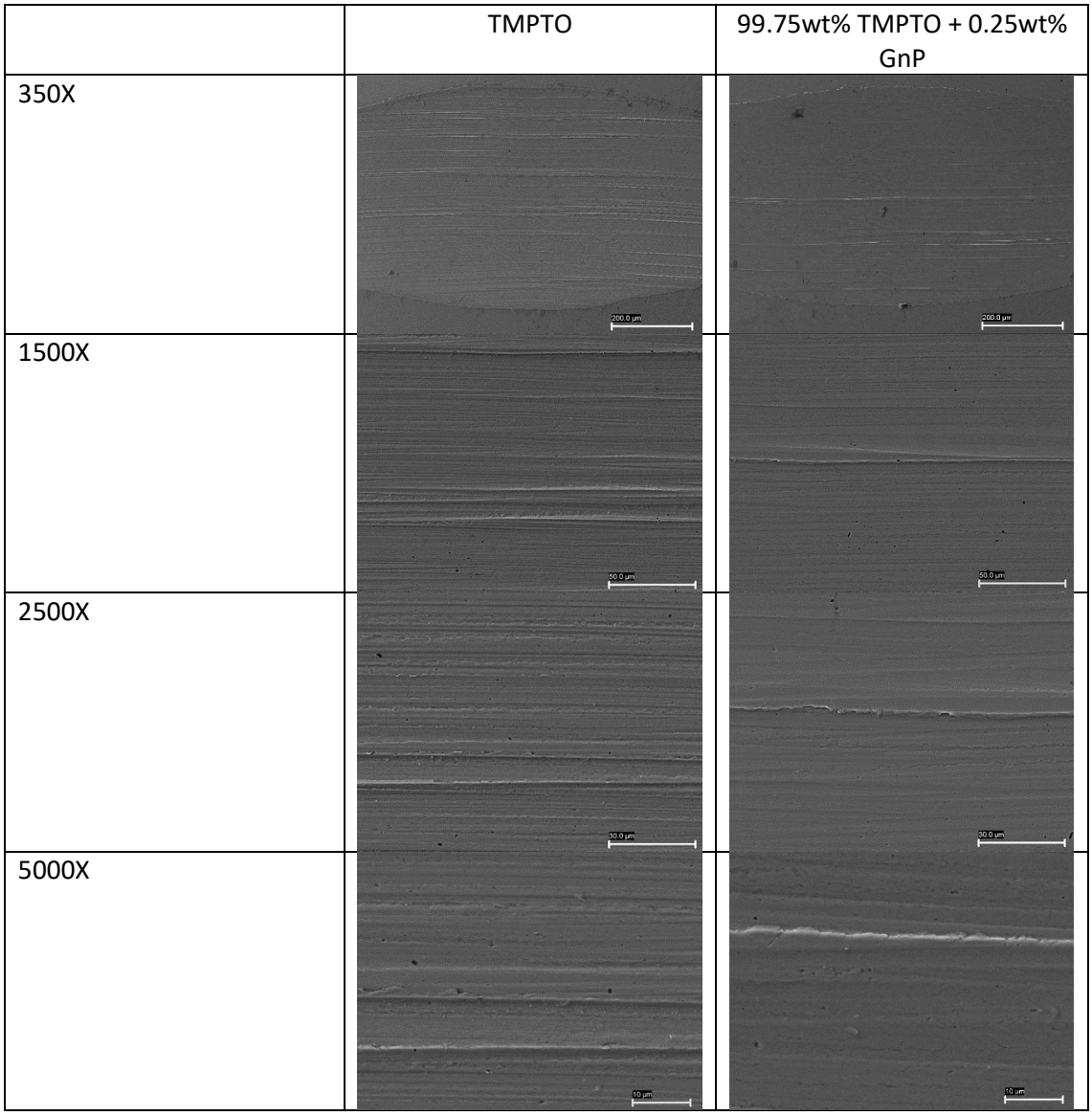

Fig. 18. SEM images of the wear scars on the plates lubricated with the neat TMPTO and with the 0.25 wt% GnP dispersion.

4. Conclusions

In this paper we have thermophysically characterized (in terms of density, viscosity and speed of sound) nanolubricants composed by TMPTO and GnP nanoadditives at 0.05, 0.10, 0.25 and 0.50 wt% concentrations. The two first properties increase with the addition of GnP whereas the speed of sound very slightly diminishes when concentration increases. Viscosity is the property more influenced by the GnP concentration, reaching increases closed to 11% for the

highest concentration respect to the pure base oil TMPTO. The three properties were successfully correlated as functions of both temperature and volume fraction by means of simple empirical equations.

Adiabatic compressibility and acoustic impedance were determined from the speed of sound and density data, the former decreasing with nanoparticle concentration whereas the latter increases. From the analysis of the acoustical properties and the FTIR spectra, it is shown that no chemical interactions between TMPTO and GnP are presented, but there being only physical interactions between nanoparticles and the neat oil.

The friction coefficient was for all the nanolubricants lower than that obtained with pure TMPTO. The minimum wear width was obtained for the nanolubricant with a 0.25 wt% in GnP. Thus, the best combined antiwear and antifriction performance corresponds to this concentration.

Acknowledgments

We would like to thank REPSOL and Croda for providing our laboratory with the TMPTO sample. This work was supported by Spanish Ministry of Economy and Competitiveness and the ERDF programme through ENE2014-55489-C2-1-R and ENE2017-86425-C2-2-R projects. Moreover, this work was funded by the Xunta de Galicia (AGRUP2015/11 and GRC ED431C 2016/001). The three last funders also financed the acquisition of the 3D Optical Profile Sensofar S Neox (UNST15-DE-3156). JMLR acknowledges Xunta de Galicia for a Principia contract.

5. References

[1] H. Spikes, Tribol. Lett. 60 (2015) 1.
[2] S. Shahnazar, S. Bagheri, S.B.A. Hamid, Int. J. Hydrogen Energy 41 (2016) 3153.
[3] A.K. Hussein, Renew. Sust. Energ. Rev. 42 (2015) 460.
[4] S.B. Koppula, N.V.V.S. Sudheer, Int. J. Appl. Eng. Res. 11 (2016) 3509.
[5] P.K. Das, J. Mol. Liq. 240 (2017) 420.
[6] Z.J. Zhang, D. Simionesie, C. Schaschke, Lubricants 2 (2014) 44.
[7] D. Guo, G. Xie, J. Luo, J. Phys. D: Appl. Phys. 47 (2014).

[8] M. Sgroi, F. Gili, D. Mangherini, I. Lahouij, F. Dassenoy, I. Garcia, I. Odriozola, G. Kraft, Tribol. Trans. 58 (2015) 207.
[9] P.U. Aldana, F. Dassenoy, B. Vacher, T.L. Mogne, B. Thiebaut, A. Bouffet, Tribol. Trans. 59 (2016) 178.
[10] M. Mehrali, E. Sadeghinezhad, S.T. Latibari, S.N. Kazi, M. Mehrali, M.N.B.M. Zubir, H.S.C. Metselaar, Nanoscale Res. Lett. 9 (2014) 15.
[11] A.K. Rasheed, M. Khalid, W. Rashmi, T.C.S.M. Gupta, A. Chan, Renew. Sust. Energ. Rev. 63 (2016) 346.
[12] G.D. Bellis, A. Tamburrano, M. Mulattieri, M.S. Sarto, 12th IEEE International Conference on Nanotechnology (IEEE-NANO), Birmingham, United Kingdom 2012.
[13] E. Sadeghinezhad, M. Mehrali, R. Saidur, M. Mehrali, S.T. Latibari, A.R. Akhiani, H.S.C. Metselaar, Energy Convers. Manage. 111 (2016) 466.
[14] M.B. Moghaddam, E.K. Goharshadi, M.H. Entezari, P. Nancarrow, Chem. Eng. J. 231 (2013) 365.
[15] P. Dhar, M.H.D. Ansari, S.S. Gupta, V.M. Siva, T. Pradeep, A. Pattamatta, S.K. Das, J. Nanopart. Res. 15 (2013) 2095.
[16] E. Sadeghinezhad, H. Togun, M. Mehrali, P.S. Nejad, S.T. Latibari, T. Abdulrazzaq, S.N. Kazi, H.S.C. Metselaar, Int. J. Heat Mass Transf. 81 (2015) 41.
[17] S.S.N. Azman, N.W.M. Zulkifli, H. Masjuki, M. Gulzar, R. Zahid, J. Mater. Res. 31 (2016) 1932.
[18] M. Vakili, S. Khosrojerdi, P. Aghajannezhad, M. Yahyaei, Int. Commun. Heat Mass Transf. 82 (2017) 40.
[19] S. Iranmanesh, H.C. Ong, B.C. Ang, E. Sadeghinezhad, A. Esmaeilzadeh, M. Mehrali, J. Clean. Prod. 162 (2017) 121.
[20] W. Rashmi, M. Khalid, Y.L. Xiao, T.C.S.M. Gupta, G.Z. Arwin, J. Eng. Sci. Technol. 12 (2017) 365
[21] V. Eswaraiah, V. Sankaranarayanan, S. Ramaprabhu, ACS Appl. Mater. Interfaces 3 (2011) 4221.
[22] D. Berman, A. Erdemir, A. V.Sumant, Carbon 54 (2013) 454.
[23] Y.-B. Guo, S.-W. Zhang, Lubricants 4 (2016) 30.
[24] A.K. Rasheed, M. Khalid, A. Javeed, W. Rashmi, T.C.S.M. Gupta, A. Chan, Tribol. Int. 103 (2016) 504.
[25] L. Wu, L. Gu, Z. Xie, C. Zhang, B. Song, Ceram. Int. 43 (2017) 14218.
[26] S.S.K. Kiu, S. Yusup, V.S. Chok, A. Taufiq, R.N.M. Kamil, S. Syahrullail, B.L.F. Chin, Mater. Sci. Eng. 206 (2017) 012043.
[27] Y. Wu, W. Li, X. Wang, Lubr. Sci. 27 (2015) 369.
[28] I. Otero, E.R. López, M. Reichelt, J. Fernández, Tribol. Int. 70 (2014) 104.
[29] E. Beran, M. Łoś, A. Kmiecik, J. Synth. Lubr. 25 (2008) 75.
[30] Y. Wu, W. Li, M. Zhang, X. Wang, Thermochim. Acta 569 (2013) 112.
[31] S. Qiao, Y. Shi, X. Wang, Z. Lin, Y. Jiang, Energy & Fuels 31 (2017) 7185.
[32] M. Mehrali, S.T. Latibari, M. Mehrali, T.M.I. Mahlia, H.S.C. Metselaar, M.S. Naghavi, E. Sadeghinezhad, A.R. Akhiani, Appl. Therm. Eng. 61 (2013) 633.
[33] X. Zhang, S. Wan, J. Pu, L. Wang, X. Liu, J. Mater. Chem. 21 (2011) 12251.
[34] Y. Hao, Y. Wang, L. Wang, Z. Ni, Z. Wang, R. Wang, C.K. Koo, Z. Shen, J.T.L. Thong, Small 6 (2010) 195.
[35] A.C. Ferrari, Solid State Communications 143 (2007) 47.
[36] A.C. Ferrari, J. Meyer, V. Scardaci, C. Casiraghi, M. Lazzeri, F. Mauri, S. Piscanec, D. Jiang, K. S Novoselov, S. Roth, A.K. Geim, Raman Spectrum of Graphene and Graphene Layers. 2006.
[37] D. Graf, F. Molitor, K. Ensslin, C. Stampfer, A. Jungen, C. Hierold, L. Wirtz, Nano Letters 7 (2007) 238.
[38] B. Tang, h. Guoxin, H. Gao, Appl. Spectrosc. Rev. 45 (2010) 369.
[39] F. Novotny-Farkas, W. Böhme, H. Stabinger, W. Belitsch, Anton Paar World Tribology Congress II, 2001.

[40] X. Paredes, O. Fandiño, M.J.P. Comuñas, A.S. Pensado, J. Fernández, J. Chem. Thermodyn. 41 (2009) 1007.
[41] F.M. Gaciño, T. Regueira, L. Lugo, M.J.P. Comuñas, J. Fernández, J. Chem. Eng. Data 56 (2011) 4984.
[42] M.J.P. Comuñas, J.-P. Bazile, A. Baylaucq, C. Boned, J. Chem. Eng. Data 53 (2008) 986.
[43] S. Kannaiyan, C. Boobalan, A. Umasankaran, A. Ravirajan, S. Sathyan, T. Thomas, J. Mol. Liq. 244 (2017) 469.
[44] K. Khanafer, K. Vafai, Int. J. Heat Mass Transf. 54 (2011) 4410.
[45] B.C. Pak, Y.I. Cho, Exp. Heat Transf. 11 (1998) 151.
[46] E. Pop, V. Varshney, A.K. Roy, MRS Bull. 37 (2012) 1273.
[47] E.J. Wasp, J.P. Kenny, R.L. Gandhi, Solid-liquid flow slurry pipeline transportation. 1st edn. Trans.Tech. Publications, Germany, 1977.
[48] D. Yoon, Y.-W. Son, H. Cheong, Nano Lett. 11 (2011) 3227.
[49] V.Y. Rudyak, Adv. Nanopart. 2 (2013) 266.
[50] V.Y. Rudyak, A.V. Minakov, Eur. Phys. J. E 41 (2018) 15.
[51] C.A. Angell, in: K. Ngai, G.B. Wright (Eds.), Relaxation in Complex Systems, US Dpt of Commerce, Springfield, 1985.
[52] C.A. Angell, Science 267 (1995) 1924.
[53] K.R. Harris, M. Kanakubo, L.A. Woolf, J. Chem. Eng. Data 52 (2007) 1080.
[54] G.K. Batchelor, J. Fluid Mech. 83 (1977) 97.
[55] H. Chen, Y. Ding, C. Tan, New J. Phys. 9 (2007) 367.
[56] M.J.G. Guimarey, M.R. Salgado, M.J.P. Comuñas, E.R. López, A. Amigo, D. Cabaleiro, L. Lugo, J. Fernández, J. Mol. Liq. 262 (2018) 126.
[57] E.R. López, J.L. Daridon, F. Plantier, C. Boned, J. Fernández, Int J Thermophys 27 (2006) 1354.
[58] B.M. Roehner, Physica A 348 (2005) 659.
[59] A.K. Kasar, P.L. Menezes, Int. J. Adv. Manuf. Technol. 97 (2018) 3999.
[60] T. Akagaki, K. Kato, Wear 117 (1987) 179
[61] G. Plint, STLE 70th Annual Meeting & Exhibition, Dallas, TX, USA, 2015.
[62] R. Pamies, M.D. Avilés, J. Arias-Pardilla, T. Espinosa, F.J. Carrión, J. Sanes, M.D. Bermúdez, Tribol. Int. 122 (2018) 200.
[63] Z. Liu, H. Wei, B. Tang, S. Xu, Z. Shufen, Sol. Energ. Mat. Sol. C. 174 (2018) 538.
[64] V. Zin, S. Barison, F. Agresti, L. Colla, C. Pagura, M. Fabrizio, RSC Adv. 6 (2016) 59477.
[65] M. Farsadi, S. Bagheri, N.A. Ismail, J. Mol. Liq. 244 (2017) 304.
[66] B. Gupta, N. Kumar, K. Panda, S. Dash, A.K. Tyagi, Sci. Rep. 6 (2016) 18372.
[67] L. Liu, Z. Fang, A. Gu, Z. Guo, Tribol. Lett. 42 (2011) 59.
[68] M. Gulzar, H.H. Masjuki, M.A. Kalam, M.V. ., N.W.M. Zulkifli, R.A. Mufti, R. Zahid, J. Nanopart. Res. 18 (2016) 223.
[69] M. Akbulut, J .Powder Metall. Min. 1 (2012) 1000e101.
[70] S. Choudhary, H.P. Mungse, O.P. Khatri, J. Mater. Chem. 22 (2012) 21032.
[71] B.M. Kamel, A. Mohamed, M.E. Sherbin, K.A. Abed, M. Abd-Rabou, J. Dispersion Sci. Technol. 38 (2017) 1495.

Supplementary Information

Thermophysical and tribological properties of dispersions of graphene in a trimethylolpropane trioleate based oil

José M. Liñeira del Río[a], María J. G. Guimarey[a], María J. P. Comuñas[a], Enriqueta R. López[a,*], Alfredo Amigo[b], Josefa Fernández[a]

[a]Laboratory of Thermophysical Properties, Nafomat Group, Department of Applied Physics, Faculty of Physics, University of Santiago de Compostela, 15782, Santiago de Compostela, Spain

[b]Laboratory of Thermophysical and Superficial Properties of liquids, Department of Applied Physics, Faculty of Physics, University of Santiago de Compostela, 15782, Santiago de Compostela, Spain

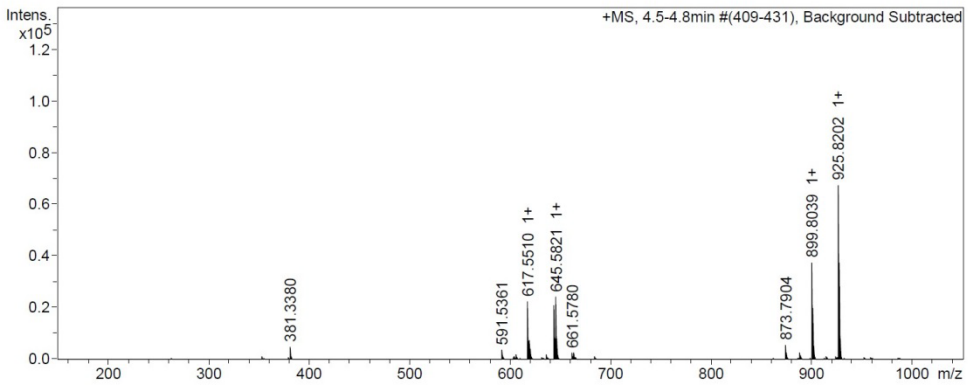

Fig. S1. Mass spectrum of the base oil compound (component 2 in Fig. 3) with one C=C bond more than TMPTO.: Retention time 4.7 min

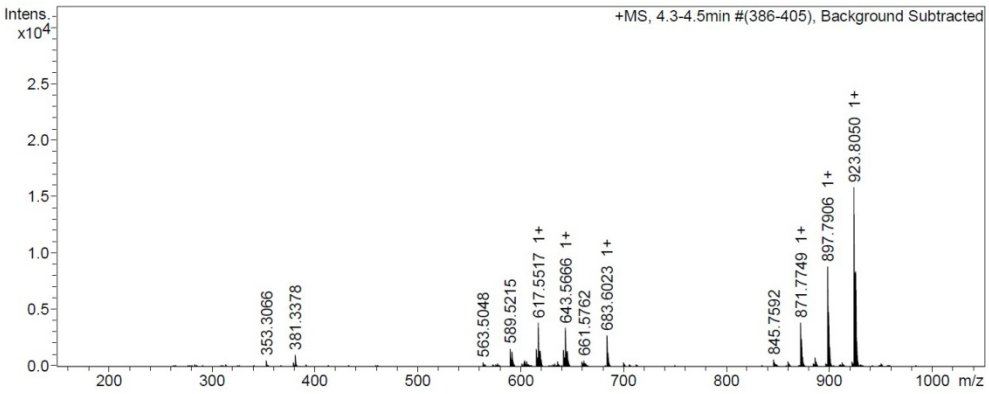

Fig. S2. Mass spectrum of the base oil compound (component 1 in Fig. 3) with two C=C bonds more than TMPTO. Retention time 4.4 min